ICAS-88-3.11R2

FLOW FIELD VISUALIZATION STUDY ON A 65° DELTA WING

K.A. Bütefisch
DFVLR - Institut für Experimentelle Strömungsmechanik,
34 Göttingen, Germany

Abstract

The aim of this study is to provide experimental flow field data on a delta wing with rounded leading edge for a better understanding of the physical behavior of the flow field which is strongly dominated by the formation, development and decay of vortices. For this purpose complementary to force, pressure, and velocity measurements the flow was visualized by means of the laser light sheet and the oil flow technique. The 420 mm chord model of MBB was tested at a Mach number of $M_\infty = 0.85$ and angles of attack of $\alpha = 10°, 20°$, and 25° in the 1 x 1 m² Transonic Wind Tunnel TWG of the DFVLR. The Reynolds number based on model chord was $Re = 4.5 \cdot 10^6$. The development of the primary and secondary vortical system has been observed, sudden changes of the structure of the flow field have been found, and by means of a digital image processing system quantitative data of the positions of the vortices have been obtained.

Introduction

In recent years much work was done to develop powerful numerical codes to predict the rather complex flow field of delta wings, especially at higher angles of attack. Usually the results of the computational work are compared with experimental results obtained by pressure and force measurements. Although agreement has been found to some extent at lower angles of attack the state of the art is unsatisfactory. Since comparisons are made on the basis of the global data the influence of local flow properties as the formation of vortices remains unknown.

In order to collect as many experimental data as possible for comparison with numerical results, the International Vortex Flow Experiment, a joint US/European program between FFA, US AFWAL, NLR, TU Delft, MBB, Dornier, DFVLR, and TU Braunschweig was initiated. Within this program flow visualization tests at M=0.85 have been performed at the DFVLR Göttingen in addition to force, pressure, and three component LDA velocity measurements [1,2,3]. The flow visualization tests were conducted as far as possible simultaneously in a combined manner. An overview of the whole experimental program is given in Ref. 4.

Wind tunnel and model

The Transonic Wind Tunnel TWG of the DFVLR Göttingen [5] is a continuous closed circuit tunnel. The transonic test section operates in the Mach number range from $M_\infty = 0.50$ to 1.20 at total pressures ranging from 0.25 to 1.6 bar. The test section has a cross section of 1m². It is enclosed in a plenum chamber which houses the laser and the optical components for flow visualization.

The model is a 0.8 scaled model of the AFWAL-model [6], and was manufactored by MBB. The root chord length C is 420 mm. The sweep angle is 65°. At x/C = 0.85 the wing is cut off. As the tests are performed at high angles of attack the model is supported by a cranked sting. Fig.1 shows the model positioned close to the center of the window of the transonic test section. The beams of the 3 component LDA system and, in the background, the X-beam construction for the support of the optical system can be seen.

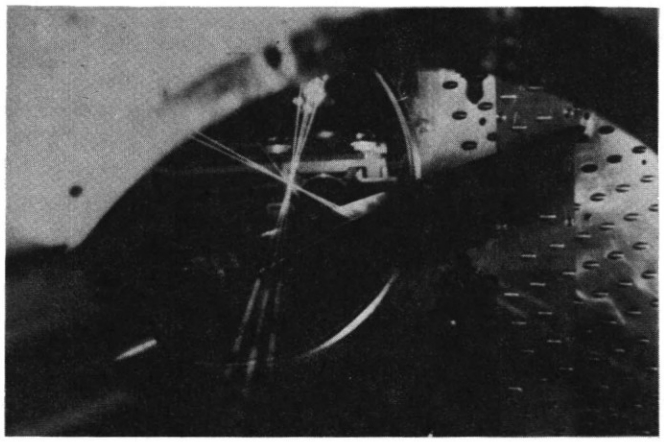

Fig. 1: Delta wing model in the 1 x 1 m^2 Transonic Wind Tunnel TWG, DFVLR Göttingen.

Careful calibration of the sting support provided for correcting the angle of attack during a run. Due to the lift the vertical position of the model is changed up to about 10 mm. Therefore the positions of two marks at the fuselage of the model have been measured before and during the run. From the measured displacement of the two marks within the xz-plane the real angle was derived. The actual position of the model was obtained within an error of $\pm$ 0.1*mm*.

Laser sheet technique

Flow visualization was performed using the laser of the laser Doppler anemometer, passing the total laser power by means of an additional mirror along the middle axis of the LDA set-up onto a cylindrical lens to form the laser light sheet. By rotating the cylindrical lens in

accordance with the angle of attack a sheet perpendicular to the model surface was illuminated. The lens was rotated by a small remotely controlled servo-motor. The optical axis of the whole device was oriented perpendicular to the main flow direction. Due to the constraints of space in the plenum chamber of the tunnel, the overall set-up was limited to a total length of 1.40 m which was also the minimum length given by the 4 W argon ion laser (Spectra Physics Mod. 165).

The whole optical system was mounted on a coordinate table to permit traversing along the axis of the model in steps of 10 to 20 mm. The specific measuring stations, at which the laser sheet should be positioned during a run, were preselected and stored in the computer before the test took place. Controlled by the computer, the desired positioning of the laser sheet was performed automatically. The laser power had to be reduced in some cases to about 1W. Since the plenum pressure was only about 60% of the atmospheric pressure, the laser had to be adjusted by remote control, otherwise the laser ceased to lase.

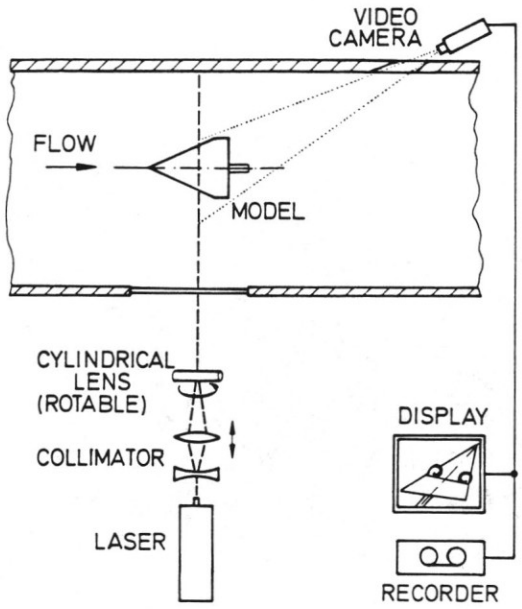

Fig. 2: Experimental set-up for the flow visualization by laser sheet technique.

A small but very powerful video-camera with CCD sensor and a focal length of 10 mm was used. The overall sensitivity was about $7 \cdot 10^{-3}$ lux. The camera was attached outside of the wall of the test section, Fig. 2. Through one hole of the side wall pictures of the illuminated flow field were taken and recorded by a video recorder.

In some tests the camera was placed behind the model on the sting. But unfortunately due to the small size of the smoke particles the scattered light intensity in directions perpendicular to the laser beam direction was quite low according to Mie's scattering law.

Smoke was generated by a disco smoke generator. The advantage of such a device is that the smoke generation can be quickly switched on and off and that the smoke disappears immediately after passing the test section. The probe for inserting the smoke was installed in the settling chamber and its position in a plane perpendicular to the main flow direction was remotely controlled.

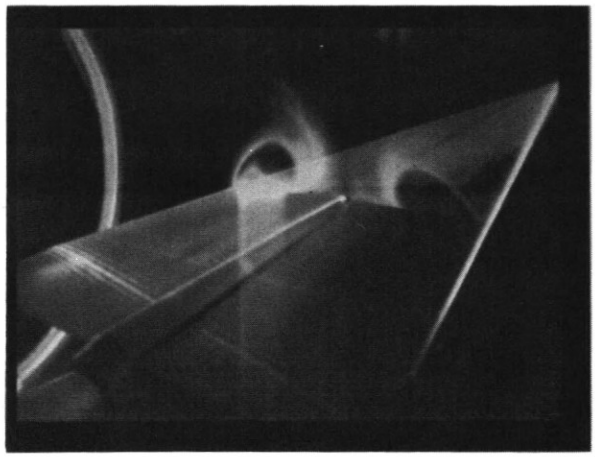

Fig. 3: Primary and secondary vortices visualized by the laser sheet technique.

Fig. 3 shows a typical result of visualizing the vortex system above the wing. As the camera was positionned at the side wall the pictures are distorted. But the structure of the wing vortex and the secondary vortex can be seen. In addition to qualitative information about the structure of the flow field usually taken from flow visualization pictures quantitative results were obtained by the use of a digital image processing system [7]. Each video frame under test was digitized and different procedures were applied to extract the desired quantities.

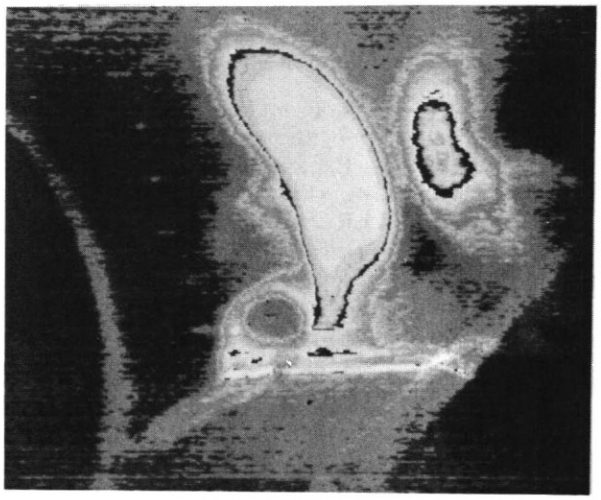

Fig. 4: Nearly concentrically arranged brightness pattern of the vortex area visualized by an image processing system.

As already mentionned the flow visualization pictures are distorted. For comparison with other flow field results the individual pixels of the pictures have to be transformed into a cross plane normal to the model surface, but for the present study it was sufficient to account for the oblique coordinate system in the video pictures.

As shown in Fig. 4 different grey values indicate equally spaced brightness intervalls. Assuming that these correspond to equally spaced smoke densities which in turn are assumed to be distributed along equal levels of velocity gradients a rough description of the geometric structure of the vortex is obtained. The different grey values are arranged almost concentrically. It seems to be reasonable to attribute the center of the smallest area to the vortex axis.

The flow visualization technique can be run in different modes. One mode is to traverse the light sheet along the chord of the wing, the angle of incidence held fixed. By rotating the cylindrical lens of the laser light sheet optics the light sheet can always be aligned perpendicular to the surface of the model. The second mode of operation is to hold the position of the laser light sheet fixed and to change the angle of attack of the model. Running this mode the plane of the light sheet is held fixed at an intermediate position, so that a perpendicular orientation of the sheet with respect to the surface of the model is not always attained. Since the maximum angle of attack is 25° the deviation does not exceed 12.5°.

In the modes of operation discussed above the smoke is inserted into the flow at an almost fixed position. Merely for optimization purposes small corrections of the position are made. On the other hand the capability of positioning the smoke insertion provides a third mode of operation for the visualization system. By this technique different areas of the flow field can be visualized. Inserting the smoke in the tip region of the wing only the flow field of the tip region is visualized. If the position of the smoke insertion is further moved into the direction of the mid plane the vortices on both sides of the wing become visible. It should be mentionned that in each case the smoke is distributed non-uniformely. So far the brightness and the shape of the pictures are fluctuating and the quality of the individual frames of the video tape may change. Nevertheless as long as the flow is steady the visualizated structures remain unaffected.

Development of vortices at higher angle of attack

Fig. 3 shows typical results for an angle of attack of $\alpha \approx 20°$. For $x/C \approx 0.60$ the main and secondary vortices are present. The above mentioned image processing scheme was applied to the video pictures which were obtained for an angle of attack of $\alpha = 20°$. From all the video pictures taken along the cord the spanwise positions of the center of the primarary and the secondary vortex core are plotted in Fig. 5. Although the data show a certain amount of scatter a straight line may be drawn through the positions of the primary vortex starting at the apex of the wing. This result agrees quite well with the result of pressure measurements, [1, 8], Fig. 6. The formation of the secondary vortices starts further downstream.

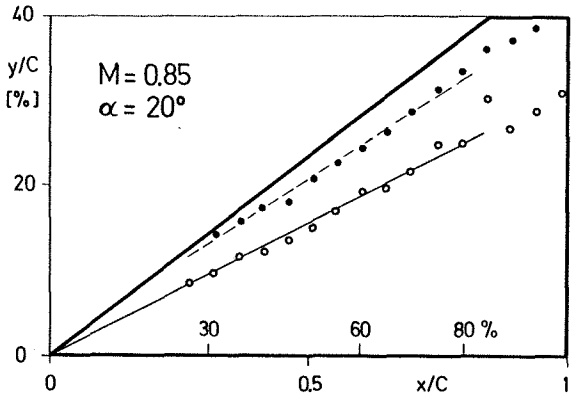

Fig. 5: Positions of primary and secondary vortices in chordwise direction; $\alpha = 20°$.

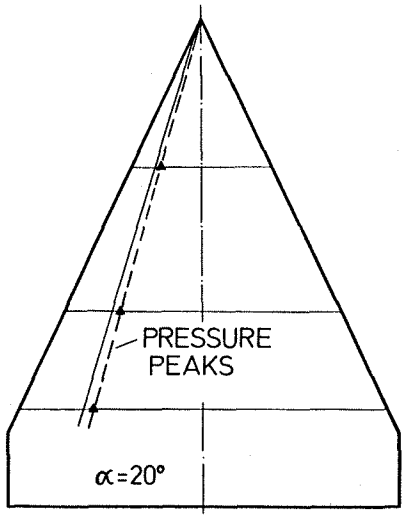

Fig. 6: Chordwise position of the primary vortex in comparison with results from pressure measurements; $\alpha = 20°$.

The distribution of the smoke allows to determine a mean diameter D of the vortices. Fig. 7 depicts the dependence of the vortex diameter on the relative root chord distance x/C. The diameter is increasing linearly refering to a conical behavior of the flow. Close to the trailing edge a sudden jump of the diameter is found, which is perhaps due to the clipping of the delta wing. In Fig. 8 the vortex diameter related to the local semispan S along the root chord length is plotted. A value around $D/S \sim 0.40$ is found and shows an increase for x/C > 0.70.

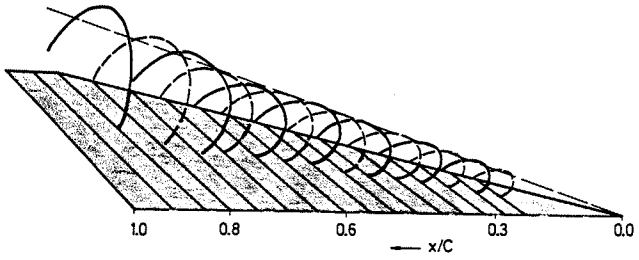

Fig. 7: Dependence of the effective diameter on the root chord length; $\alpha = 20°$.

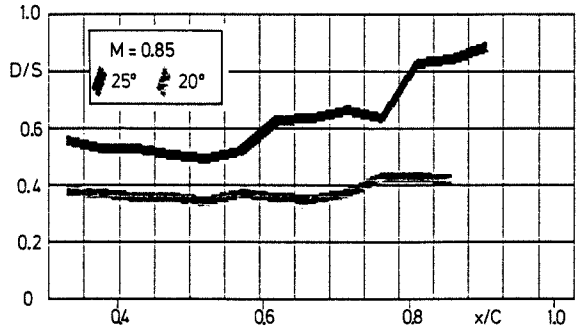

Fig. 8: Dependence of the relative vortex diameter on the root chord length for $\alpha = 20°$ and $25°$.

If the angle of attack is increased to $\alpha = 25°$ the change of the vortex diameter in chord wise direction is no longer linear. Already at $x/C \sim 0.6$ a sudden jump is observed, Fig. 9. Around x/C = 0.80 a second enhencement of the cross sectional area is found. In comparison with the case of $\alpha = 20°$ the relative vortex diameter D/S is increased. For x/C < 0.60 the value is around 0.50, Fig. 8. For x/C > 0.80 the value is twice the value obtained for the smaller angle of attack.

A similar behavior of the development of the flow in chord wise direction is visible in the photograph of the oil surface flow visualization, [1]. For x/C > 0.60 the lines of the separation and reattachement indicate a dramatic change of the flow conditions. Also Euler code calculations [9] predict for x/C > 0.60 a considerable deviation of the position of the vortex axis, Fig. 10. Moreover these observations coincide with the findings of pressure measurements, [1,8], where the pressure distributions show a sudden loss in the suction peak level for the most downstream wing section.

Careful examination of the video tape provides also information about the temporal behavior of the flow field. As the resolution in time is 20 msec (50 semi frames per second) low frequency fluctuations of the flow become visible. For x/C < 0.60 the shape of the vortex is quite

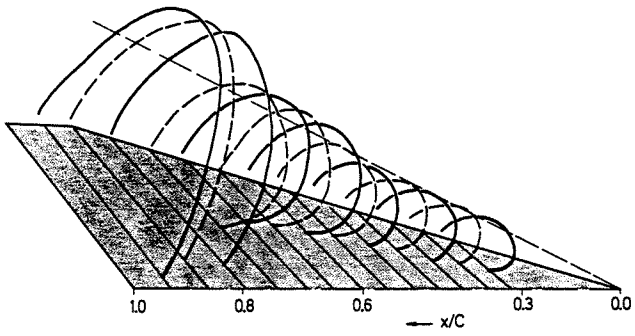

Fig. 9: Dependence of the effective diameter on the root chord length; $\alpha = 25°$.

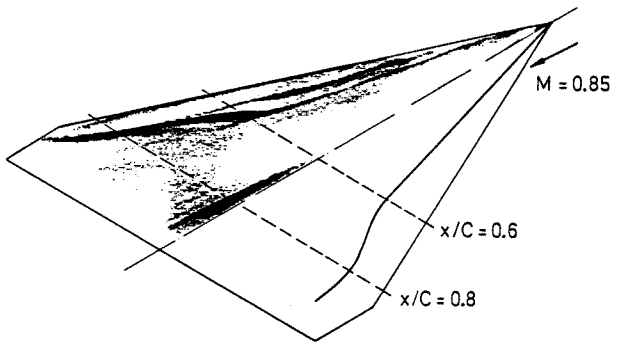

Fig. 10: Results of oil surface flow visualization and Euler computation for vortex break-down.

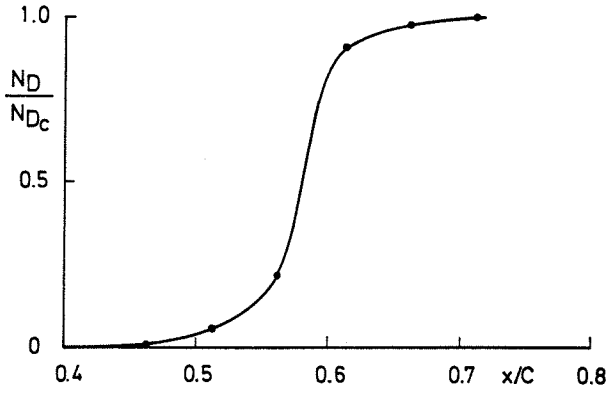

Fig. 11: Temporal occurrance of enlarged vortex diameter in the case of vortex break-down.

stable. In addition to the primary vortex a secondary vortex can be seen. A small distance further downstream the effective diameter seems to jump between two values. At first the diameter corresponds to the conical behavior of the flow but with increasing x/C the enlarged diameter is observed more frequently. In Fig. 11 the temporal occurrence of the larger diameter D relative to the occurence of the "conical" diameter D_c is plotted in chord wise direction. For x/C > 0.60 the larger diameter is preponderant in accordance with the jump in Fig. 8.

The sudden change of the flow characteristics is interpreted as vortex break-down. In addition to the sudden change of the size of the vortex the flow visualization by the laser light sheet technique offers a further significant indication for vortex break-down: A stable vortex has a dark core area as only a very small amount of smoke penetrates near the apex into the vortical core area and is subsequentely distributed over the increasing vortex core. From the outer vortex sheets no smoke is able to enter into the core area. After vortex bursting occurs the turbulence within the vortex area is increasing and flow reversal is expected [10]. Smoke from the outer and downstream region enters into the core region and makes it visible. Fig. 12 shows the vortex system above the wing for an angle of attack $\alpha = 25^{\circ}$ and at a position x/C = 0.80. In contrast to Fig. 3 the central area of the vortex is filled up with smoke.

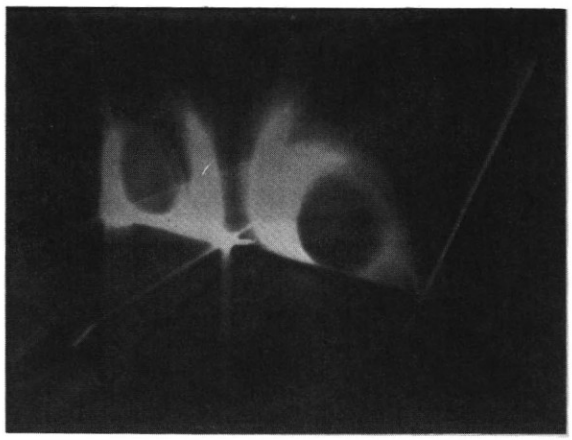

Fig. 12: Vortex for $\alpha = 25^{\circ}$. Due vortex break-down the central area is filled with smoke.

Development of the vortices with increasing incidence

If the angle of attack is very small the flow visualization by the laser light sheet technique does not give any information about the flow field. Merely the stream line becomes visible in which the smoke has been inserted upstream of the model. The smoke filled area is fluctuating due to the turbulence of the incoming flow. Possibly the fluctuations are caused by the insertion of the smoke into the flow field of the settling chamber.

For x/C =0.60 and an incidence of $\alpha = 4.0^{\circ}$ a small black area, Fig. 13, very close to the tip occurs indicating the beginning of separation and vortex formation. With increasing incidence the flat area becomes larger and is growing mainly in normal direction. The curvature of the bubble close to the tip is caused by the flow coming around the tip. The curvature at the inboard side provides information on the reattachment process. At lower incidence the apparent reattachment angle between the visible smoke sheet and the surface is below 90°. With increasing incidence the angle is also increasing and finally exceeds 90° .

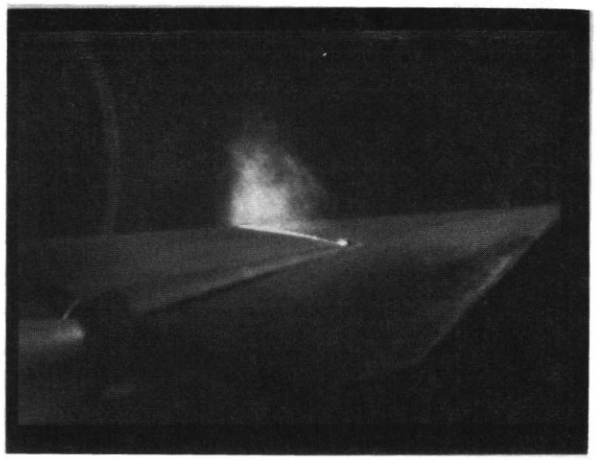

Fig. 13: Beginning of separation and vortex formation for $\alpha = 4^{\circ}$.

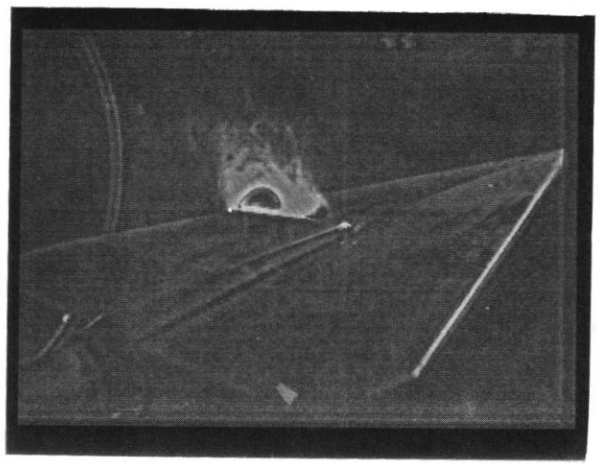

Fig. 14 Additional structure close to the mid plane.

It is difficult to detect the beginning of the formation of the secondary vortex. But by observing carefully the sequence of video frames before the second vortex is clearly visible a limiting value for the corresponding angle of attack is found. It seems that then the apparent reattachment angle exceeds 90° .

The improvements which have been made on the laser light sheet technique during the last years result in a greatly improved quality of the flow field pictures. Furthermore the application of a digital image processor allows to enhence structures of interest [7]. Using this improved technique at an angle of attack of $\alpha = 10^{\circ}$ and x/C = 0.60 in addition to the primary and secondary vortices a structure separated from this well known system is detected, Fig. 14. It disappears if the angle of attack is increased and is not visible if the secondary vortex is well developed. This inboard structure has not been observed at the 80% wing section.

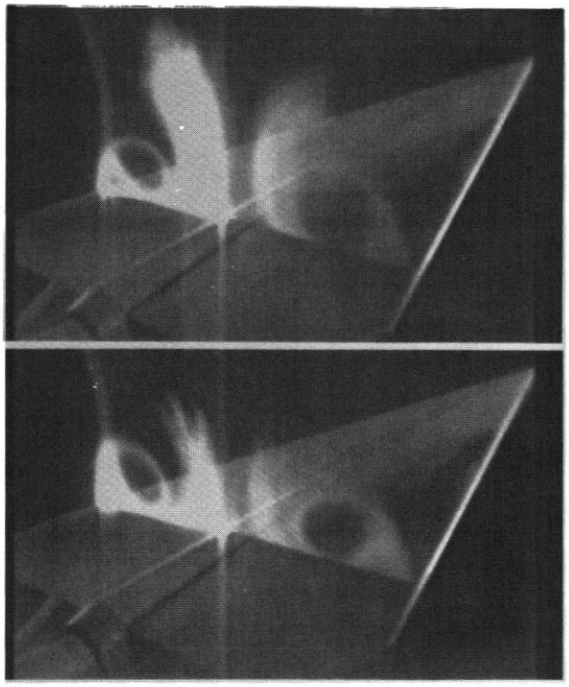

Fig. 15: Sudden change from one stable vortical structure to another at the 80% wing section.

If the incidence is increased the secondary vortex is clearly distinguishable from the main vortex. Even in the case of vortex break-down no change of the configuration is noticed although Fig. 11 indicates the fluctuation of the vortex diameter. Possibly the starting position in chordwise direction of the vortex break-down changed after the perforated walls of the wind tunnel were replaced by slotted walls.

Looking at the 80% wing section the dramatic change of the vortical structure is observed when the angle of incidence is changed only little: From one video frame to the next the shape jumps from the stable configuration to the vortex break-down configuration, Fig. 15. The corresponding angle of attack is different whether the angle is increased or decreased, e.g. a typical hysteresis behavior of the vortex break-down has been found.

The results extracted from the visualization pictures are plotted in the tentative view of the flow development of Ref. 8, Fig. 16. The results of Ref. 8 are deduced from pressure measurements and schlieren photographs. Concerning the onset of the primary vortex the results agree closely, but regarding the onset of the secondary vortex considerable differences are found. Following the flow visualization the secondary vortex formation begins at a smaller angle of attack. One reason may be that the pressure distribution measurement is insensitive against small local changes of the flow field. On the other hand in the flow visualization tests the Reynolds number was smaller than the pressure measurement tests. This may result in an earlier formation of the secondary vortex.

The angle of the conspicuous changes attributed to the vortex break-down agrees quite well with the angle of Ref. 8. The bursting angle depicted from the pressure measurement is found to be between the two values derived from the flow field visualization and which are due to the hysteresis effect. For the more upstream station at x/C = 0.60 the corresponding angle is $\alpha = 25°$. In the case the wind tunnel was equiped with slotted walls no significant changes of the vortical structure could be recognized, possibly indicating the sensitivity of the location of vortex break-down against wall interferences.

Conclusions

Flow field visualization on a 65° delta wing by means of the laser light sheet technique, operated at M = 0.85 in the Transonic Wind Tunnel TWG of the DFVLR Göttingen, provided successfully flow field data within the International Vortex Flow Experiment.

Although the argon ion laser, the optical components, the traversing mechanisme as well as the CCD video camera had to be installed in the plenum chamber of the wind tunnel video pictures either along the model axis or as function of the angle of attack have been obtained. Clearly the primary and the secondary vortex became visible.

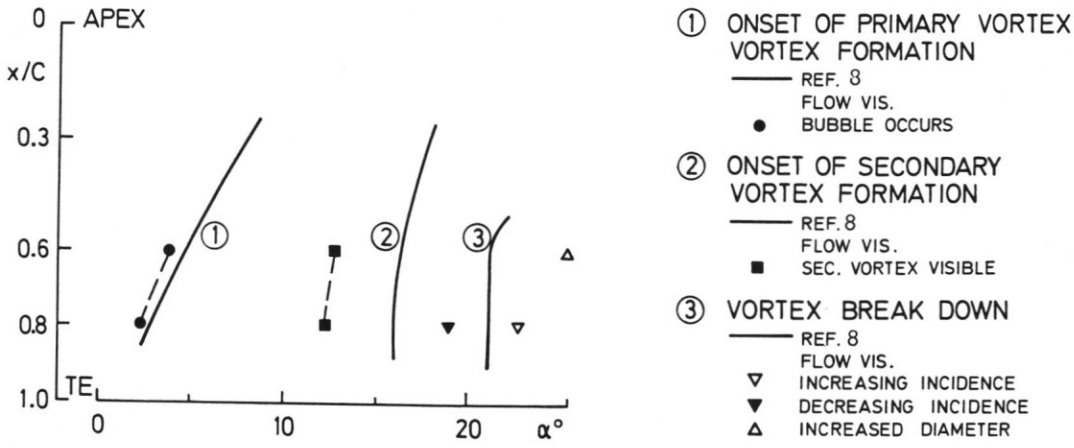

Fig. 16: Tentative view of flow development in the $x - \alpha$ plane.

Due to the use of an digital image processing system weak structures on individual frames of the video tape could be recognized. For certain flow conditions a structure in addition to the well known vortical system at the tip has been found.

Furthermore quantitative data have been derived. It was found that at an angle of attack of $\alpha = 20°$ the main vortex shows an almost conical behavior. If the angle is increased sudden changes of the vortical structure are observed and are refered to vortex break-down. The comparison of the results with the results of pressure measurements, oil surface flow visualization and numerical computation of other investigators shows a good agreement.

Acknowledgement

The DFVLR thanks MBB for the supply of the model. The experiments were carried out with the help of the DFVLR Wind Tunnel Branch (HA-WK) whose valuable contributions are gratefully acknowledged. We also want to thank Dr. K. Hartmann and Dr. E. Wedemeyer for useful discussions.
The authors are obliged to Mrs. U. Dreykluft for the preparation of the photos and figures and to Mrs. I. Nickisch for preparing the typescript.

References

1. Hartmann,K.; Force and Pressure Measurements Including Surface Flow Visualizations on a Cropped Delta Wing. "International Vortex Flow Experiment on Euler Code Validation" Symposion, FFA, Stockholm, 1986.
2. Bütefisch, K.A., Pallek, D., Sauerland, K.-H.; Three Component LDA Measurements on a 65° Delta Wing. DFVLR-Report IB 222 - 87 A 34 (1987).
3. Elsenaar, A, Eriksson, G.; Proceedings of the Symposium on the "International Vortex Flow Experiment on Euler Code Validation", Stockholm, October 1-3, 1986 (published by FFA).
4. Elsenaar, A., Hjelmberg, L., Bütefisch, K.A., Bannink, W.J.; The International Vortex Flow Experiment, AGARD Symposium on "Validation of Computational Fluid Dynamics". Lisbon, May 2-5, 1988.
5. Hottner, Th. and Lorenz-Meyer, W.; "Der Transsonische Windkanal der Aerodynamischen Versuchsanstalt Göttingen", (zweite Ausbaustufe)", Jahrbuch 1968 der WGL, 1968.
6. Boersen,S.J.; Report on Geometry of AFWAL 65° -Sweep Δ-Wing with Rounded leading Edge. NLR Memorandum AC-85-034 L, 1985.
7. Kompenhans, J.; Strömungssichtbarmachung im 3m-Niedergeschwindigkeits- Windkanal mit Hilfe der Laser Lichtschnittmethode. DFVLR-Research Report IB 222 - 86 A 29 (1986).
8. Elsenaar, A. and Bütefisch, K.A.; Experimental Study on Vortex and Shock Wave Development on a 65° Delta Wing. IUTAM Symposium Transsonicum III, DFVLR-AVA Göttingen, May 24-27, 1988.
9. Kumar, K. and Das, A.; Numerical Solution of Flow Fields Around Delta Wings Using Euler Equation Methods. "International Vortex Flow Experiment on Euler Code Validation" Symposion, FFA, Stockholm, 1986.
10. Wagner, B., Hitzel, S.M.; Computations Relating to the Vortex Flow Experiment. IUTAm Symposium Transsonicum III, DFVLR-AVA Göttingen, May 24-27, 1988.